Available online at www.sciencedirect.com
ScienceDirect
Trans. Nonferrous Met. Soc. China 28(2018) 711−721
Transactions of Nonferrous Metals Society of China
www.tnmsc.cn

Electrochemical hydrogen storage performance of as-cast and as-spun RE−Mg−Ni−Co−Al-based alloys applied to Ni/MH battery

Yang-huan ZHANG[1,2], Ya-qin LI[2,3], Hong-wei SHANG[2], Zhong-hui HOU[1,2], Yan QI[2], Dong-liang ZHAO[2]

1. Key Laboratory of Integrated Exploitation of Baiyun Obo Multi-metal Resources, Inner Mongolia University of Science and Technology, Baotou 014010, China;
2. Department of Functional Material Research, Central Iron and Steel Research Institute, Beijing 100081, China;
3. Institute for Advanced Materials and Technology, University of Science and Technology Beijing, Beijing 100083, China

Received 24 October 2016; accepted 24 April 2017

Abstract: The La−Mg−Ni−Co−Al-based AB_2-type $La_{0.8-x}Ce_{0.2}Y_xMgNi_{3.4}Co_{0.4}Al_{0.1}$ (x=0, 0.05, 0.1, 0.15, 0.2) alloys were prepared via melt spinning. The analyses of the X-ray diffraction (XRD) and scanning electron microscopy (SEM) proved that the experimental alloys contain the main phase $LaMgNi_4$ and the second phase $LaNi_5$. Increasing Y content and spinning rate lead to grain refinement and obvious change of the phase abundance without changing phase composition. Y substitution for La and melt spinning make the life-span of the alloys improved remarkably, which is attributed to the improvement of anti-oxidation, anti-pulverization and anti-corrosion abilities. In addition, the discharge capacity visibly decreases with increasing the Y content, while it firstly increases and then decreases with increasing spinning rate. The electrochemical kinetics increases to the optimum performance and then reduces with increasing spinning rate. Moreover, all the alloys achieve to the highest discharge capacities just at the initial cycle without activation.

Key words: Y; La; substitution; spinning rate; life-span; discharge capacity; electrochemical kinetics

1 Introduction

There are reports indicating that one fourth of the globe's energy consumption and 23% CO_2 emission are linked to the transport [1]. The high levels of fossil fuel consumption and greenhouse gas production have forced us to seek renewable energy as a substitute for traditional energy sources. Fortunately, a variety of sources of clean energy are stored in our planet, such as hydrogen, solar and wind. Hydrogen is the most clean and efficient energy, which is the most suitable energy to solve the above problems. However, secure storage hydrogen is still an unavoidable challenge for the implementation of hydrogen fuel vehicles. Gaseous hydrogen is known for being explosive and dangerous, and the cost of liquid hydrogen is very high. Using metal hydride storage hydrogen, by contrast, has characteristics of high efficiency, safety and so on. Unfortunately, so far there has been no one storage hydrogen alloy that can meet the requirements of Department of Energy (DOE) of USA. The major bottlenecks are the limited discharge capacity, short life-span and poor kinetics. The A_2B_7-type and AB_2-type alloys have attracted world-wide attention and research due to the discharge capacities exceeding 380 mA·h/g and relatively low production cost [2−4]. BALCERZAK et al [5] produced $La_{2-x}Mg_xNi_7$ alloys (x= 0, 0.25, 0.5, 0.75, 1) by mechanical alloying with subsequent annealing under an argon atmosphere. The electrochemical discharge capacity and gaseous hydrogen storage capacity of La−Mg−Ni alloys increase with increasing Mg content, and reach the maximum values for $La_{1.5}Mg_{0.5}Ni_7$ alloy. ZHANG et al [6] prepared the La−Mg−Ni-based A_2B_7-type $La_{0.8-x}Nd_xMg_{0.2}Ni_{3.35}$-$Al_{0.1}Si_{0.05}$ (x=0, 0.1, 0.2, 0.3, 0.4) electrode alloys. The study shows that the electrochemical kinetics of the alloy electrodes can be improved by adding suitable Nd. LIU et al [7] synthesized the $La_{0.75}R_{0.05}Mg_{0.20}Ni_{3.40}Al_{0.10}$ (R=La, Nd and Sm) alloys. They found that the electrochemical kinetics of the alloys was improved by

Foundation item: Projects (51761032, 51471054) supported by the National Natural Science Foundation of China; Project (2015MS0558) supported by the Natural Science Foundation of Inner Mongolia, China
Corresponding author: Yang-huan ZHANG; Tel: +86-10-62183115; Fax: +86-10-62187102; E-mail: zhangyh59@sina.com
DOI: 10.1016/S1003-6326(18)64703-X

substituting Nd and Sm for La partially. LI et al [8] studied the electrochemical kinetics of $La_{0.6}R_{0.2}Mg_{0.2}$-$(NiCoMnAl)_{3.5}$ (R = La, Ce, Pr, Nd) alloys and found that the maximum discharge capacity achieves to be 220 mA·h/g at 233 K and the high rate discharge (HRD) ability raises to 61.3% for the Ce-substituted alloy. WANG et al [9] synthesized $LaMgNi_4$ alloys by melt spinning, which possess discharge capacities beyond 400 mA·h/g. GUÉNÉE et al [10] proved that the $LaMgNi_4$ and $NdMgNi_4$ alloys are of cubic $MgCu_4Sn$ ($AuBe_5$-type) structure. However, the short life-span and poor kinetics have not been improved effectively up to now.

The related literatures show that the above problems can be solved by microstructure modification and alloying [11,12]. The electrochemical life-spans of the AB_2-type alloys were greatly improved through substituting La with Pr, Nd, Sm and Ce or substituting of Co, Al, Mn and Cu for Ni [13−15]. In addition, previous studies have indicated that melt spinning leads to the grain refinement and the improvement of the life-span of the A_2B_7-type alloys [16].

In this work, Y and Ce were adopted to substitute La partially. Previous studies have demonstrated that adding rare earth elements Y and Ce can effectively improve the corrosion resistance of the electrode, and further improving its electrochemical properties, especially the life-span [17]. By using the melt spinning technology, the $La_{0.8-x}Ce_{0.2}Y_xMgNi_{3.4}Co_{0.4}Al_{0.1}$ (x=0−0.2) alloys were prepared. And the influences of spinning rate and Y content on the structure and electrochemical characteristics were studied.

2 Experimental

The $La_{0.8-x}Ce_{0.2}Y_xMgNi_{3.4}Co_{0.4}Al_{0.1}$ (x=0, 0.05, 0.1, 0.15, 0.2) alloys were represented as Y_0, $Y_{0.05}$, $Y_{0.1}$, $Y_{0.15}$ and $Y_{0.2}$, respectively, depending on the Y content. And the as-cast alloys were obtained by melting the raw materials in a vacuum induction furnace. For avoiding the loss of Mg, helium was filled into the furnace at about 0.04 MPa during melting operation. A part of the cast ingots were chosen as samples and melted to obtain the as-melted alloys on the surface of a rotating copper roller. Because the cooling rate is very difficult to be precisely measured, the copper roller linear velocity is used to approximately represent the spinning rate, which was set to be 2, 6, 10 and 15 m/s, respectively.

The phase structures and compositions were identified by X-ray diffraction (XRD) with Cu $K_{\alpha 1}$ radiation filtered by graphite, and the parameters are 160 mA, 40 kV and 10 (°)/min, respectively. The morphologies were observed by scanning electron microscopy (SEM) and energy dispersive spectrometer (EDS).

The electrochemical performance was tested using a tri-electrode open system, which is made of three parts: the alloy electrode (negative electrode), the sintered $Ni(OH)_2$/NiOOH electrode (positive electrode) and the Hg/HgO electrode (reference electrode). The voltage between the negative electrode and the reference electrode is defined as the discharge voltage. The preparation of alloy electrodes is divided into the following steps: Firstly, the carbonyl nickel powder and alloy powder were mixed at a mass ratio of 4:1 with the total mass of 1 g. Secondly, the mixtures were compressed into a d15 mm wafer electrode with an electric tablet machine. Finally, the wafer electrode was encased with nickel foam and placed in a tri-electrode open cell. The tri-electrode open system was placed in the thermostat water bath in the testing process, and the temperature was controlled at (30±1) °C. According to the general electrochemical test standard, the wafer electrodes were first charged, stood for 15 min, and then discharged until the voltage up to −0.500 V at a current density of 60 mA/g.

The electrochemical impedance spectra (EIS) and the potentiodynamic polarization curves were measured using an electrochemical workstation (PARSTAT 2273). The electrodes under test were charged to 100%, stood for 2 h, and then discharged to 50% depth of discharge (DOD). It was tested and recorded 60 points per decade in the frequency range of 10 kHz−5 mHz at 5 mV of the amplitude of signal potentiostatic or galvanostatic measurements. The Tafel polarization curves were measured in the potential range of −1.2 to 1.0 V (vs Hg/HgO) at a scan rate of 5 mV/s. The potentiostatic discharge of the saturated electrode was measured by using a Corr Ware electrochemistry corrosion software (CorrWare). The test electrodes were firstly charged up and then discharged at a potential step of 500 mV for 5 ks on an electrochemical workstation.

3 Results and discussion

3.1 Microstructure characterization

Figure 1 gives the XRD patterns of the as-cast and spun $La_{0.8-x}Ce_{0.2}Y_xMgNi_{3.4}Co_{0.4}Al_{0.1}$ (x=0−0.2) alloys. The results illustrate that all alloys contain a major phase $LaMgNi_4$ and a secondary phase $LaNi_5$. In addition, the diffraction peak intensity of the $LaNi_5$ phase becomes weaken clearly, suggesting that the $LaNi_5$ phase reduces and the $LaMgNi_4$ phase increases with increasing the spinning rate and Y content. The lattice parameters of the $LaMgNi_4$ and $LaNi_5$ phases are summarized in Tables 1 and 2, which are calculated based on the XRD analysis using Jade 6.0 software and the error of calculation is <0.2%. Obviously, they reduce with increasing Y content,

while increase with increasing the spinning rate. The former is because Y has smaller atom radius than La. And the latter is ascribed to the generation of the lattice stress and crystal lattice distortion during melt spinning process.

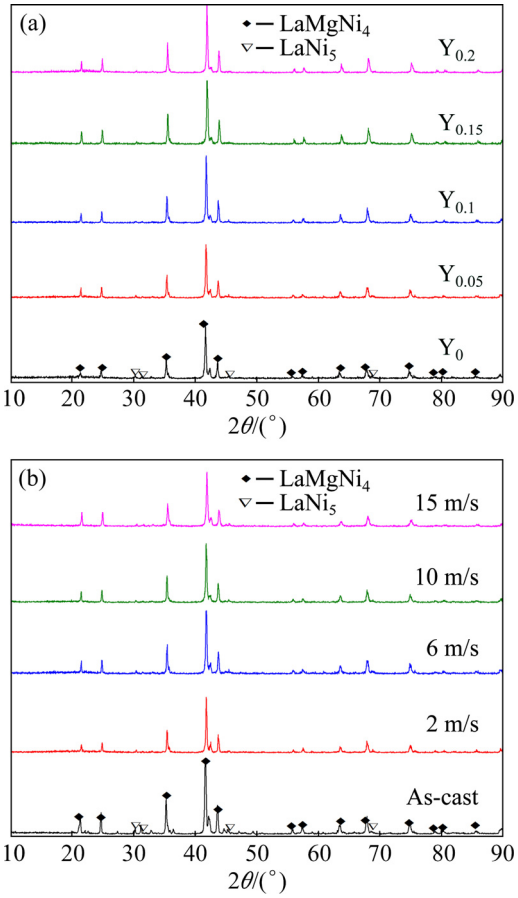

Fig. 1 XRD patterns of as-cast and as-spun $La_{0.8-x}Ce_{0.2}Y_x$-$MgNi_{3.4}Co_{0.4}Al_{0.1}$ (x=0−0.2) alloys: (a) As-spun (6 m/s); (b) $Y_{0.05}$ alloy

Table 1 Lattice constants and abundances of $LaMgNi_4$ and $LaNi_5$ phases in as-spun (6 m/s) alloys

Alloy	Phase	Lattice constant/nm		Cell volume/ nm^3	Phase abundance/ %
		a	c		
Y_0	$LaMgNi_4$	0.7182	−	0.3705	77.2
	$LaNi_5$	0.5073	0.4027	0.0897	22.8
$Y_{0.05}$	$LaMgNi_4$	0.7177	−	0.3697	78.1
	$LaNi_5$	0.5066	0.4024	0.0894	21.9
$Y_{0.1}$	$LaMgNi_4$	0.7171	−	0.3688	78.8
	$LaNi_5$	0.5061	0.4023	0.0892	21.2
$Y_{0.15}$	$LaMgNi_4$	0.7161	−	0.3672	79.3
	$LaNi_5$	0.5057	0.4019	0.0890	20.7
$Y_{0.2}$	$LaMgNi_4$	0.7152	−	0.3658	80.6
	$LaNi_5$	0.5053	0.4017	0.0888	19.4

Table 2 Lattice constants and abundances of $LaMgNi_4$ and $LaNi_5$ phases in as-spun $Y_{0.05}$ alloy

Spinning rate/($m·s^{-1}$)	Phase	Lattice constant/nm		Cell volume/ nm^3	Phase abundance/ %
		a	c		
0	$LaMgNi_4$	0.7166	−	0.3680	76.3
	$LaNi_5$	0.5058	0.4021	0.0891	23.7
2	$LaMgNi_4$	0.7173	−	0.3691	77.1
	$LaNi_5$	0.5062	0.4024	0.0893	22.9
6	$LaMgNi_4$	0.7177	−	0.3697	78.1
	$LaNi_5$	0.5066	0.4024	0.0894	21.9
10	$LaMgNi_4$	0.7179	−	0.3700	78.9
	$LaNi_5$	0.5071	0.4026	0.0897	21.1
15	$LaMgNi_4$	0.7182	−	0.3705	79.2
	$LaNi_5$	0.5077	0.4028	0.0899	20.8

Figure 2 shows the SEM images and EDS spectra of the as-cast $La_{0.8-x}Ce_{0.2}Y_xMgNi_{3.4}Co_{0.4}Al_{0.1}$ (x=0−0.2) alloys. All the alloys show a dendritic structure and obvious characteristics of the peritectic reaction with two different color regions. The EDS spectra identify that the grey region is $LaMgNi_4$ phase and the bright region is $LaNi_5$ phase. Moreover, it is also noted that the substitution of Y for La causes clear refinement of the alloy grains.

Figure 3 presents the SEM images of the as-spun $La_{0.8-x}Ce_{0.2}Y_xMgNi_{3.4}Co_{0.4}Al_{0.1}$ (x=0−0.2) alloys. It can be found that the melt spinning results in the alloy grains dramatically refining by comparing Fig. 2 with Fig. 3. In addition, the grain sizes are visibly reduced with increasing Y content and spinning rate. Also, it is noted that there are two phases in the as-spun alloys, namely the major phase $LaMgNi_4$ and secondary phase $LaNi_5$. The amount of the $LaNi_5$ phase visibly decreases with increasing spinning rate and Y content.

3.2 Electrochemical performances

3.2.1 Life-span

The capacity retaining rate (S_n) is used to measure the life-span, which can be described by formula $S_n=C_n/C_{max}\times100\%$. It is a ratio of the discharge capacity of the nth cycle (C_n) to the maximum value (C_{max}). For the alloys, the degree of capacity fade should be as low as possible. Therefore, a higher S_n value is necessary for practical application. Figure 4 presents the variations of S_n of the as-cast and as-spun $La_{0.8-x}Ce_{0.2}Y_xMgNi_{3.4}$-$Co_{0.4}Al_{0.1}$ (x=0−0.2) alloys with cycle number. The degradation rate of discharge capacity markedly slackens with increasing spinning rate and Y content, meaning significant improvement in the life-span of the alloys. To

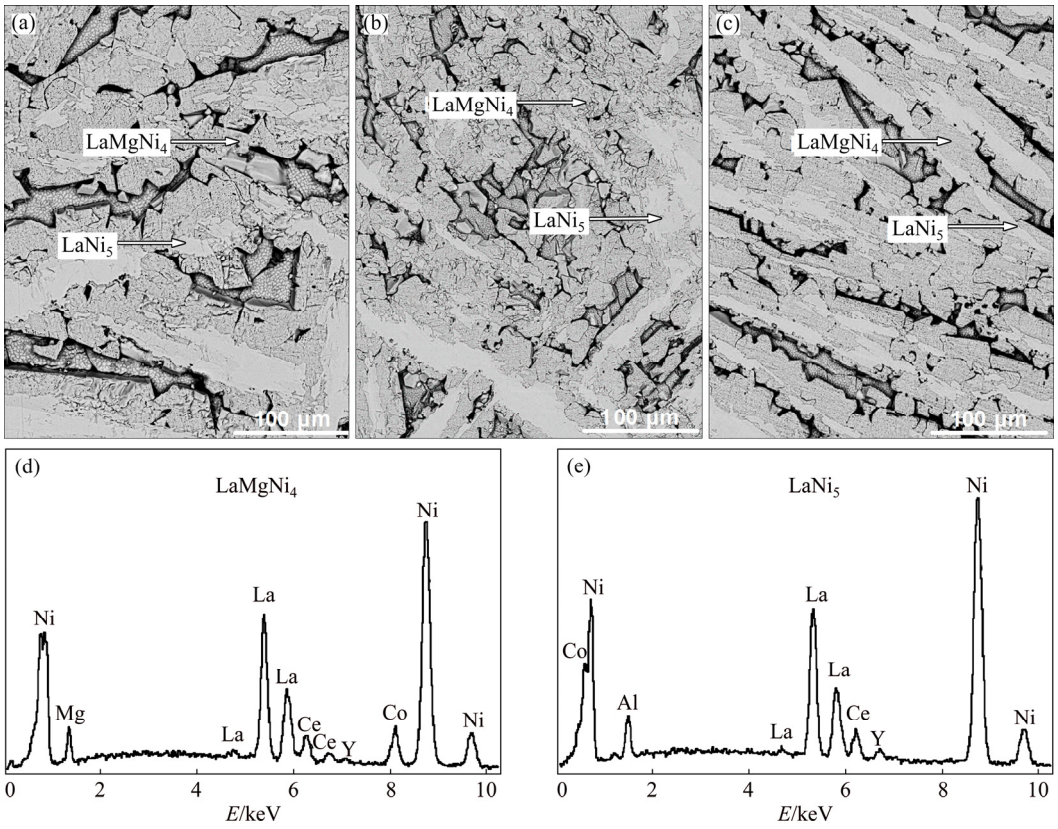

Fig. 2 SEM images (a−c) together with typical EDS spectra (d, e) of as-cast alloys: (a) Y_0 alloy; (b) $Y_{0.05}$ alloy; (c) $Y_{0.2}$ alloy

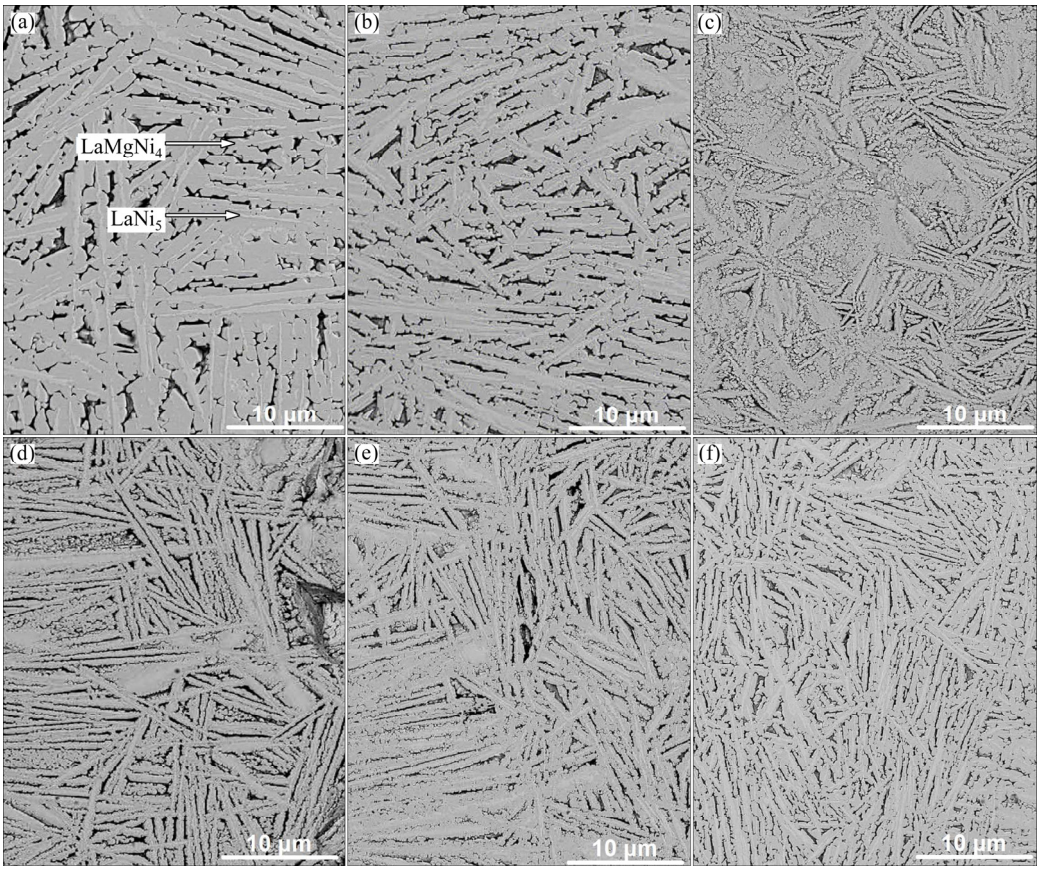

Fig. 3 SEM images of as-spun $La_{0.8-x}Ce_{0.2}Y_xMgNi_{3.4}Co_{0.4}Al_{0.1}$ (x=0−0.2) alloys: (a−c) Y_0, $Y_{0.05}$ and $Y_{0.2}$ alloys spun at 2 m/s, respectively; (d−f) $Y_{0.05}$ alloy spun at 6, 10 and 15 m/s, respectively

quantify the effects, S_{150} (n=150) values were chosen as a representative for comparison, as displayed in Fig. 4. The S_{150} value grows from 70.3% to 87.7% for the as-spun (6 m/s) alloys when Y content increases from 0 to 0.2. And the S_{150} value grows from 60.4% to 80.2% for the $Y_{0.05}$ alloys when spinning rate increases from 0 to 15 m/s.

Figure 5 displays the SEM images of the alloy particles. It is observed that hydrogenation leads to obvious changes in the morphological structure. It is worth noting that there are no any cracks before charge−discharge cycles, while a fair amount of cracks exist on the surface of the Y_0 alloy particles after that. This means that the pulverization of the alloy particles continues to worsen during the test. The reasons for the capacity fade can be summed up into two aspects. One reason is the pulverization, and the other reason is the oxidation of the alloys [18,19]. As for the former, it is caused by hydrogen atoms moving through the lattice interstitials, which causes the generation of lattice strain and lattice expansion−contraction. As for the latter, it is because the surfaces of the Y_0 alloy particles are covered by a rough and gossypine layer after electrochemical test (see Fig. 5(b)), which are identified to be $Mg(OH)_2$ and

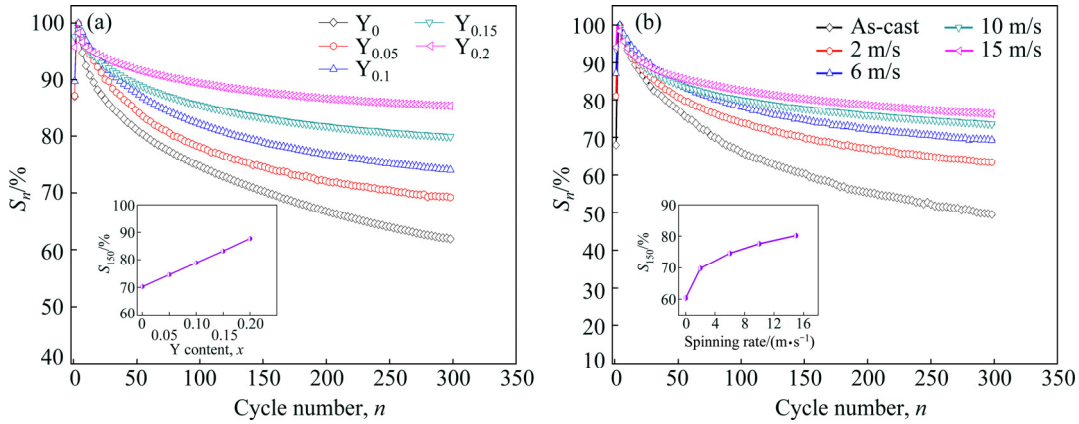

Fig. 4 Evolution of capacity retaining rate (S_n) of as-cast and as-spun $La_{0.8-x}Ce_{0.2}Y_xMgNi_{3.4}Co_{0.4}Al_{0.1}$ (x=0−0.2) alloys with cycle number: (a) As-spun (6 m/s); (b) $Y_{0.05}$ alloy

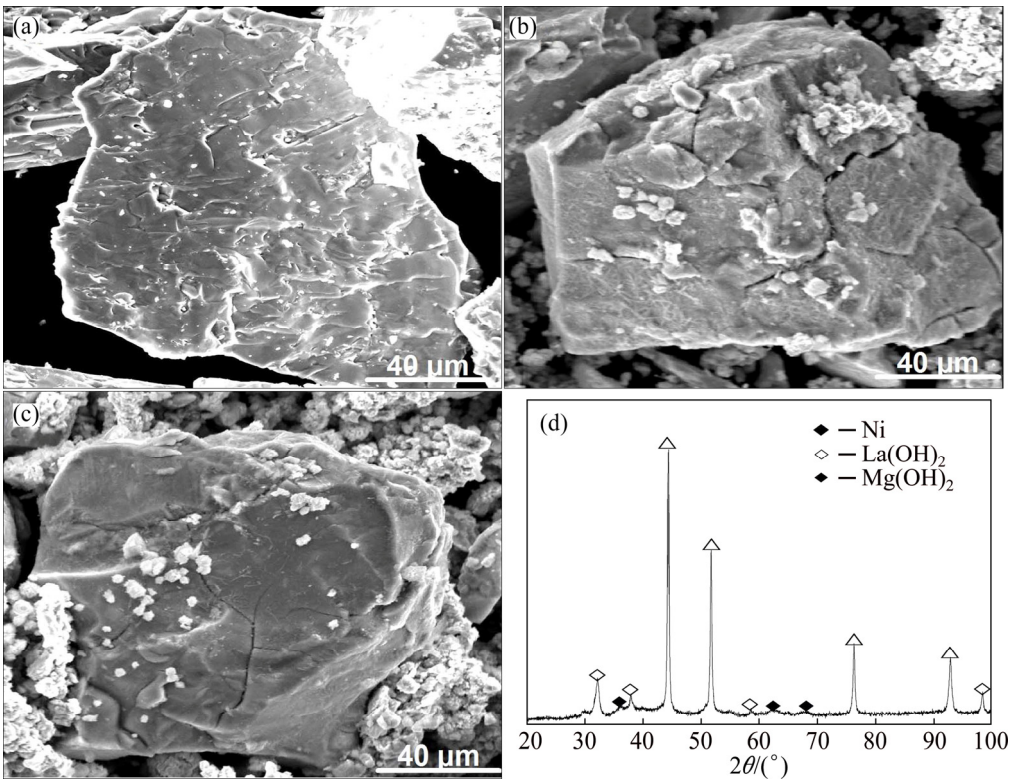

Fig. 5 SEM morphologies together with typical XRD pattern of as-spun alloys before and after electrochemical cycle: (a) As-spun (6 m/s) Y_0 alloy before cycling; (b, c) As-spun (6 m/s) Y_0 and $Y_{0.05}$ alloys after cycling, respectively; (d) XRD pattern of as-spun (6 m/s) Y_0 alloy after cycling

$La(OH)_2$ (see Fig. 5(d)). It is also worth noting that there is much less hydroxide covering $Y_{0.05}$ alloy particles, suggesting that the substitution of Y for La can reduce the corrosion rate and oxidation rate of the alloys. Therefore, we can infer from the above phenomenon that the improvement of the life-span of the alloys is ascribed to the grain refinement caused by substituting Y for La and melt spinning. The strength and toughness of the alloy increase with the decrease of grain size. In other words, the smaller the size of alloy grain is, the better its strength and toughness will be, meaning that the higher the anti-pulverization capability will be.

3.2.2 Discharge potential characteristic, discharge capacity and activation capability

Figure 6 displays the discharge potential curves of the as-cast and as-spun $La_{0.8-x}Ce_{0.2}Y_xMgNi_{3.4}Co_{0.4}Al_{0.1}$ (x=0−0.2) alloys. The output powder of a battery is determined by the discharge potential characteristics. And the discharge potential plateau should be as long and horizontal as possible. It is verified that the discharge potential is enhanced and the discharge plateau is lengthened by substituting La with Y and melt spinning. Furthermore, it is observed that the variations of the spinning rate and Y content have important effects on the discharge capacity, as described in Fig. 6. Apparently, increasing Y content is adverse to the improvement of the discharge capacity of the as-spun alloys, as shown in Fig. 6(a). Specifically, it decreases from 371.5 to 353.7 mA·h/g when Y content increases from 0 to 0.2. However, increasing the spinning rate has affirmative and negative impacts on the discharge capacity. It firstly increases to 379.9 mA·h/g and then decreases, as given in Fig. 6(b).

Figure 7 displays the discharge capacity curves of the as-cast and as-spun $La_{0.8-x}Ce_{0.2}Y_xMgNi_{3.4}Co_{0.4}Al_{0.1}$ (x=0−0.2) alloys. Here, n is the cycle number corresponding to the maximum discharge capacity. For applying in Ni/MH battery, n should be as small as possible. It is evident that the samples can reach their peak values of the discharge capacity at the initial cycle, suggesting that the samples possess excellent activation capability. It can be concluded from the above analyses that increasing Y content and spinning rate have significant effects on the electrochemical performance

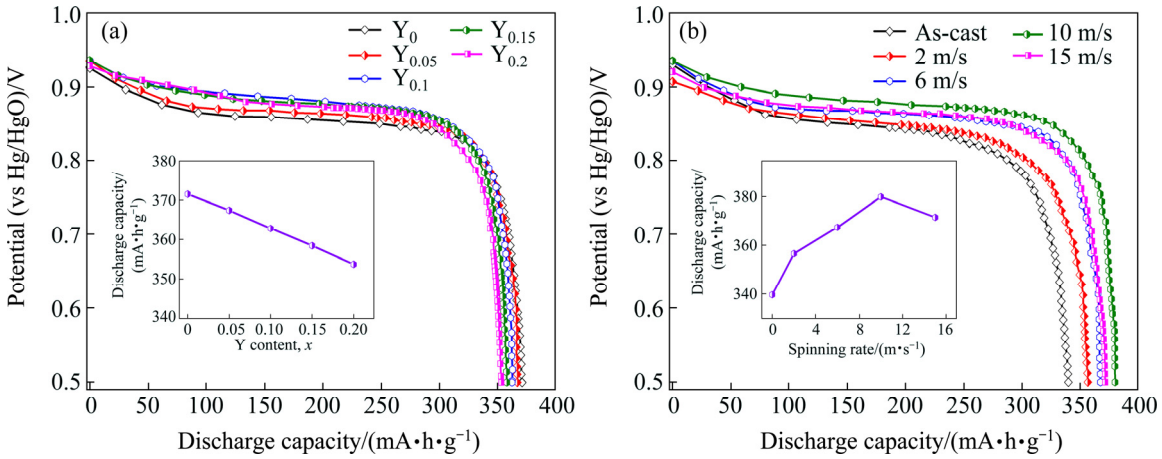

Fig. 6 Discharge potential curves of as-cast and as-spun $La_{0.8-x}Ce_{0.2}Y_xMgNi_{3.4}Co_{0.4}Al_{0.1}$ (x=0−0.2) alloys: (a) As-spun (6 m/s); (b) $Y_{0.05}$ alloy

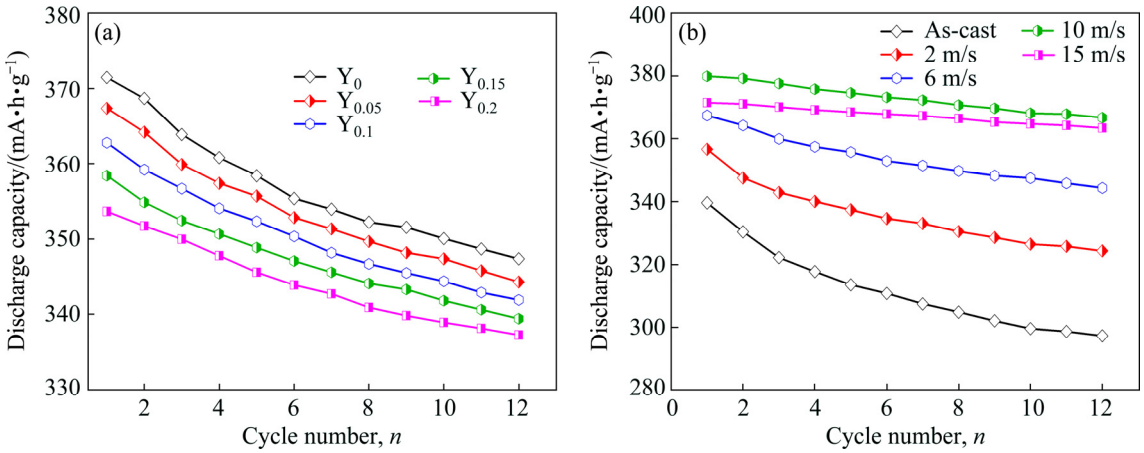

Fig. 7 Evolution of discharge capacity of as-cast and as-spun $La_{0.8-x}Ce_{0.2}Y_xMgNi_{3.4}Co_{0.4}Al_{0.1}$ (x=0−0.2) alloys with cycle number: (a) As-spun (6 m/s); (b) $Y_{0.05}$ alloy

and structure. As for the potential characteristic, it depends on the ohmic internal resistance and polarization resistance. The former is almost the same for all of the alloys because it reflects the contact resistance and the latter appears different values because it is inversely proportion to the diffusion coefficient D [20]. The positive effects of Y substitution for La and melt spinning on the potential characteristics are most probably ascribed to the grain refinement because the grain boundaries can be served as the diffusion access for hydrogen atoms [21]. As for the discharge capacity, it depends on the grain size, phase composition, surface state, composition uniformity and crystal structure, etc. The negative impact of substituting Y for La on discharge capacity is closely related to the reduction of the cell volume because the discharge capacity is proportional to the cell volume. In addition, it achieves the maximum capacity at spinning rate of 10 m/s and then decreases, meaning that melt spinning has both positive and negative effects on the discharge capacity. The positive role is the grain refinement caused by melt spinning because the grain boundary can store more hydrogen than other regions [22]. The negative role is associated with the generation of the lattice stress during melt spinning because the lattice stress will hinder the proceeding of electrochemical reactions. As for the superior activation capability, it is principally associated with multiphase structures because the phase boundary can be viewed as the buffer zone to relieve the lattice distortion and lattice strain formed in the process of electrochemical testing. In addition, the grain refinement caused by melt spinning and Y substitution for La is also beneficial to improving the activation capability.

3.2.3 Electrochemical kinetics

The high rate discharge ability (η_{HRD}), which can be described by formula $\eta_{HRD}=C_J/C_{60}\times100\%$, reflects the kinetics of the alloy electrode. It is a ratio of the discharge capacity at the current density of J (C_J) to that at 60 mA/g (C_{60}). Figure 8 displays the changing trend of the η_{HRD} values of the as-cast and as-spun $La_{0.8-x}Ce_{0.2}Y_x$-$MgNi_{3.4}Co_{0.4}Al_{0.1}$ (x=0−0.2) alloys with different current densities. Obviously, it declines with increasing the current density. For comparison, J=300 mA/g is taken as a representative, and the relationships between the η_{HRD} and Y content and spinning rate are inserted in Figs. 8(a) and (b), respectively. The η_{HRD} firstly increases to 97.5% for the as-spun (6 m/s) alloy and 95.3% for the $Y_{0.05}$ alloy, but decreases gradually with further increasing Y content or spinning rate respectively.

The control factors of kinetics can be summed up into two aspects. One reason is the hydrogen diffusion ability in the bulk of the alloys, and the other reason is charge-transfer rate on the surfaces of the alloy electrodes [23]. The latter can be calculated by measuring the electrochemical impedance spectrum (EIS) according to the Kuriyama's model [18]. Figure 9 shows the typical representative of EIS curves. It can be seen in Fig. 9 that each curve contains a large capacitive loop, a small capacitive loop and a line, which commendably describes the electrochemical reaction of the electrode materials. The small capacitive loop reflects the contact

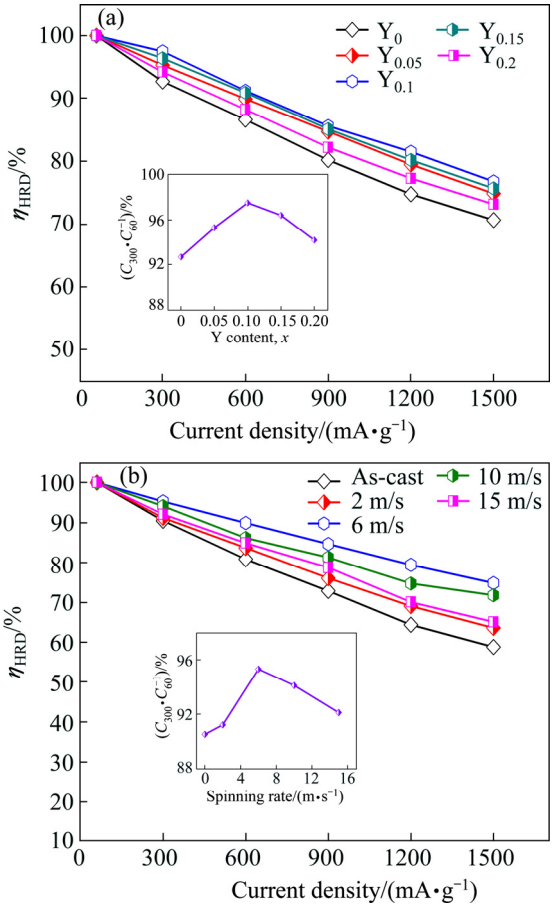

Fig. 8 Evolution of η_{HRD} of as-cast and as-spun $La_{0.8-x}Ce_{0.2}$-$Y_xMgNi_{3.4}Co_{0.4}Al_{0.1}$ (x=0−0.2) alloys with current density: (a) As-spun (6 m/s); (b) $Y_{0.05}$ alloy

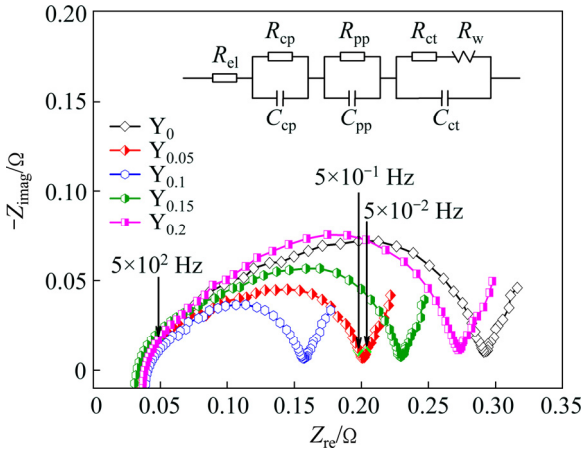

Fig. 9 Electrochemical impedance spectra (EIS) of as-spun (10 m/s) $La_{0.8-x}Ce_{0.2}Y_xMgNi_{3.4}Co_{0.4}Al_{0.1}$ (x=0−0.2) alloys and equivalent circuit

resistance between the alloy powders and conductive materials, the larger one reflects the charge transfer resistance (R_{ct}) on the alloy surface, whereas the straight line reflects Warburg impendence. It can be obtained by fitting the experimental results based on the equivalent circuit (see Fig. 9). As considered by KURIYAMA et al [18], the R_{ct} value principally depends on both the reactivity of the alloy surface and reaction area. And the former can be determined by apparent activation enthalpy $\Delta_r H^*$, which can be obtained by the following equation [19]:

$$\ln(T/R_{ct}) = C_0 - \frac{\Delta_r H^*}{RT} \quad (1)$$

where R_{ct} is the charge transfer resistance, R is the mole gas constant, T is the thermodynamic temperature of the sample and C_0 is a constant in which the surface area is included.

Considering the calculation conditions of Eq. (1), the EIS curves of the as-cast and as-spun $La_{0.8-x}Ce_{0.2}Y_xMgNi_{3.4}Co_{0.4}Al_{0.1}$ (x=0−0.2) alloys are measured at 303, 318, and 333 K. As a representative, the EIS curves of the as-spun (6 m/s) $Y_{0.05}$ and $Y_{0.1}$ alloys are shown in Fig. 10. Based on the data of Fig. 10, the Kuriyama graphs of $\ln(T/R_{ct})$ vs $1/T$ can be plotted by using logarithmic transform of Eq. (1), as inserted in Figs. 10(a) and (b). According to the slopes of the Kuriyama plots, $\Delta_r H^*$ values can be calculated easily. Thus, the relationships between the $\Delta_r H^*$ value and spinning rate and Y content are given in Fig. 11. The $\Delta_r H^*$ values firstly decrease and then increase with increasing spinning rate and Y content. This implies that the melt spinning and substituting Y for La have two-sided influence on the charge transfer rate. As for the substitution of Y for La, the positive impact is most likely related to the improvement of the corrosion resistance, which inhibits the progress of the oxidation reactions of La and Mg [24]. In addition, it also causes the generation of the Ni-rich layer on the surfaces of the alloys, thus enhancing the electrocatalytic activity of the electrodes. The negative impact is most likely related to the grain refinement because it can slow the

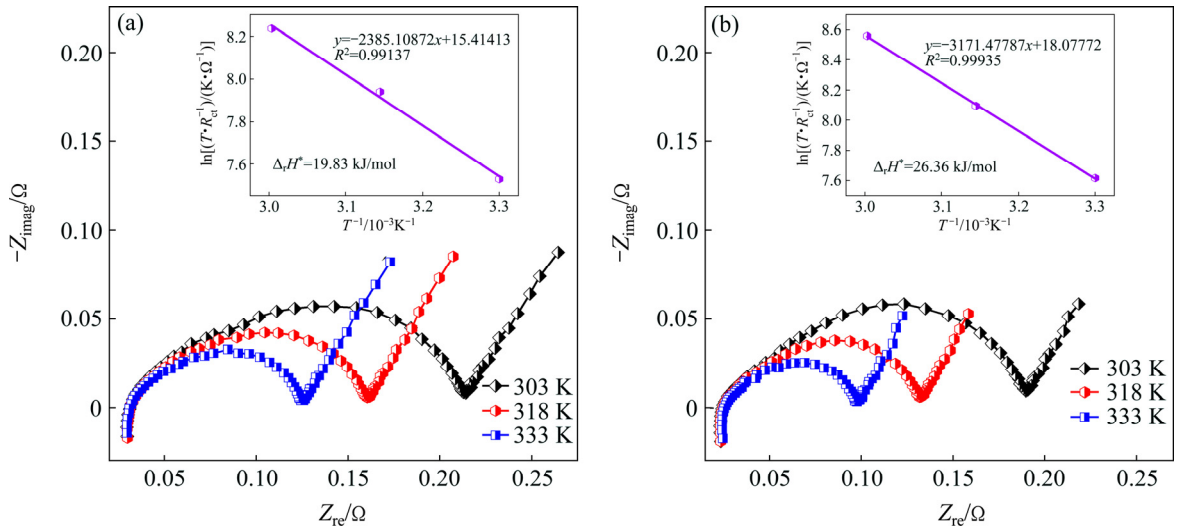

Fig. 10 Electrochemical impedance spectra (EIS) curves of as-spun (6 m/s) $Y_{0.05}$ (a) and $Y_{0.1}$ (b) alloys at various temperatures

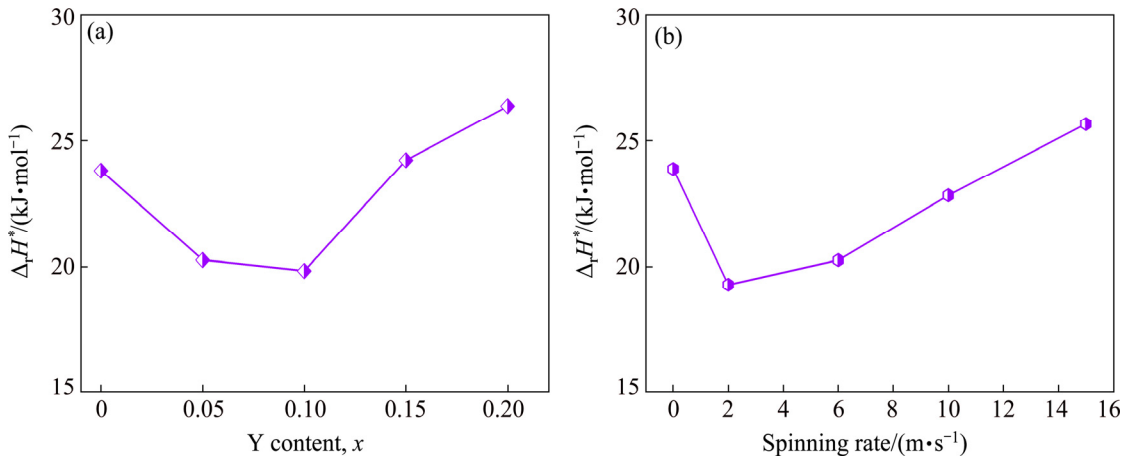

Fig. 11 Evolution of activation enthalpy $\Delta_r H^*$ values of $La_{0.8-x}Ce_{0.2}Y_xMgNi_{3.4}Co_{0.4}Al_{0.1}$ (x=0−0.2) alloys with Y content and spinning rate: (a) As-spun (6 m/s); (b) $Y_{0.05}$ alloy

pulverization progress of the alloys and the generation of the new surface, further influencing charge transfer rate [25]. As for the melt spinning, the positive impact is most likely related to the generation of crystallographic characteristics. KLEPERIS et al [26] believe that the crystallographic and electronic structures are the main driving forces for the charge-transfer rate of an alloy electrode. The negative impact is considered to be the result of the ultra-refined grains.

Figure 12 shows the semilogarithmic curves of anodic current vs the working duration of an alloy electrode. The diffusion coefficient D could be obtained based on the slope of the linear region by the following formulae [27]:

$$\lg J = \lg\left(\pm\frac{6FD}{da^2}(C_0 - C_s)\right) - \frac{\pi^2}{2.303}\frac{D}{a^2}t \quad (2)$$

$$D = -\frac{2.303a^2}{\pi^2}\frac{\mathrm{d}\lg J}{\mathrm{d}t} \quad (3)$$

where D denotes the hydrogen diffusion coefficient (cm^2/s), J denotes the diffusion current density (A/g), d denotes the density of the hydrogen storage alloy (g/cm^3), a denotes the alloy particle radius (cm), t denotes the discharge time (s), C_0 denotes the initial hydrogen concentration in the bulk of the alloy (mol/cm^3), and C_s denotes the hydrogen concentration on the surface of the alloy particles (mol/cm^3). The functional relations of D values and spinning rate and Y content are inserted in Fig. 12. Obviously, the D values firstly rise and then decrease with increasing spinning rate and Y content.

Figure 13 displays the potentiodynamic polarization curves of the electrodes. A similar turnover point exists in each curve. The corresponding current density is termed as the limiting current density (J_L), suggesting that oxidation reactions occur on the alloy electrode surface, and the formed oxidation layers restrain the hydrogen atoms diffusion [14]. The variation tendencies of the D and J_L values with spinning rate and Y content are very similar through comparing Fig. 12 and Fig. 13, namely increasing firstly and then decreasing with increasing spinning rate and Y content. The variation trend is the same as that of the η_{HRD} vulues, meaning that the diffusion ability is the most fundamentally

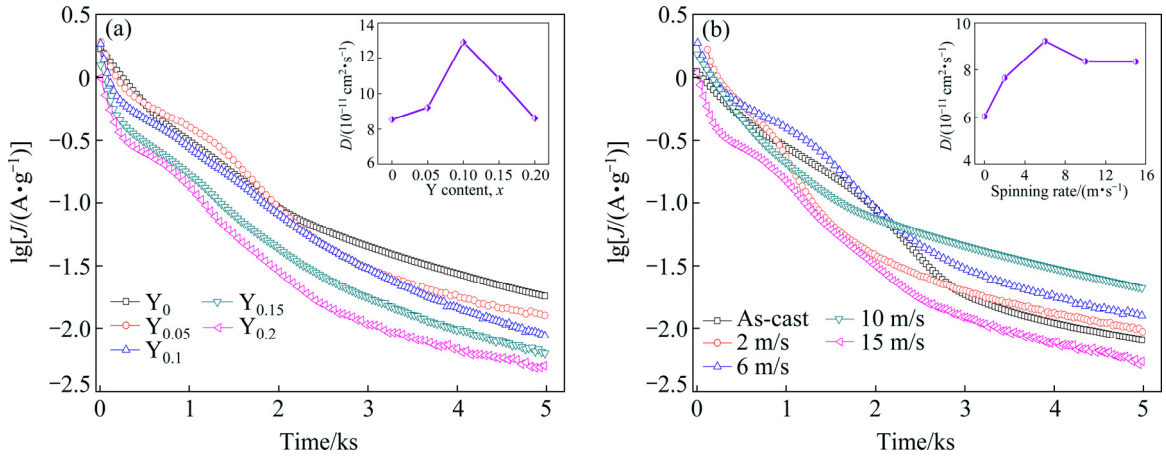

Fig. 12 Semilogarithmic curves of anodic current density vs time of as-cast and as-spun $La_{0.8-x}Ce_{0.2}Y_xMgNi_{3.4}Co_{0.4}Al_{0.1}$ (x=0−0.2) alloys: (a) As-spun (6 m/s); (b) $Y_{0.05}$ alloy

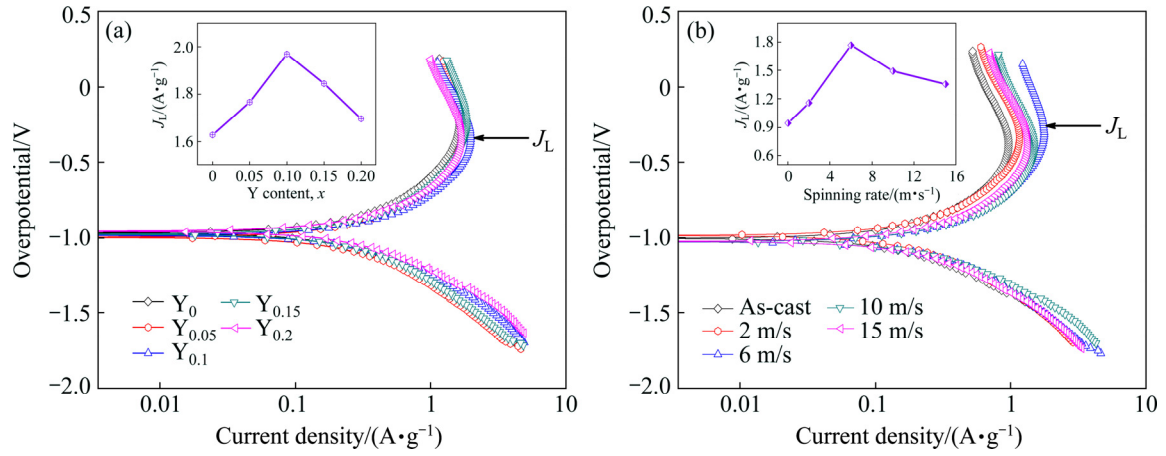

Fig. 13 Potentiodynamic polarization curves of as-cast and as-spun $La_{0.8-x}Ce_{0.2}Y_xMgNi_{3.4}Co_{0.4}Al_{0.1}$ (x=0−0.2) alloys: (a) As-spun (6 m/s); (b) $Y_{0.05}$ alloy

determinant of the electrochemical kinetics for the electrodes. The grain refinement can evidently enhance the diffusion ability of hydrogen atoms, which has been mentioned previously. The adverse effects are mainly reflected in the decrease of the cell volume due to the fact that the reduction in the lattice constants and the cell volume will increase the needed diffusion activation energy of hydrogen atoms, consequently impairing hydrogen diffusion [28]. The negative impact on hydrogen diffusion caused by melt spinning is most probably associated with the generation of the lattice distortion, which leads to the increase of diffusion activation energy.

4 Conclusions

1) The structure characterization of the as-cast and as-spun $La_{0.8-x}Ce_{0.2}Y_xMgNi_{3.4}Co_{0.4}Al_{0.1}$ (x=0−0.2) reveals that the melt spinning and substituting Y for La result in an increase in $LaMgNi_4$ phase and a decrease in $LaNi_5$ phase without altering the phase compositions of the alloys. And the melt spinning and the substituting of Y for La make the alloy grains obviously refined. Moreover, the substitution of Y for La leads to the decrease of the lattice parameters and cell volumes of the alloys visibly, whereas the melt spinning generates an exactly opposite result.

2) The electrochemical tests show that the melt spinning and the substitution of Y for La are in favor of improving the anti-pulverization, anti-corrosion and anti-oxidation abilities of alloys, further improving the electrochemical life-span of the alloys. The discharge capacity of the alloys visibly decreases with increasing Y content, while there exists the maximum value with increasing spinning rate.

3) The electrochemical kinetics of the as-cast and as-spun alloys firstly increases and then decreases with increasing spinning rate and Y content, for which the structure modified is principally responsible. The hydrogen diffusion is the main controlling factor of the high rate discharge ability of the alloys.

References

[1] MORI D, HIROSE K. Recent challenges of hydrogen storage technologies for fuel cell vehicles [J]. International Journal of Hydrogen Energy, 2009, 34: 4569−4574.

[2] LI R F, XU P Z, ZHAO Y M, WAN J, LIU X F, YU R H. The microstructures and electrochemical performances of $La_{0.6}Gd_{0.2}Mg_{0.2}Ni_{3.0}Co_{0.5-x}Al_x$ (x=0−0.5) hydrogen storage alloys as negative electrodes for nickel/metal hydride secondary batteries [J]. Journal of Power Sources, 2014, 270: 21−27.

[3] KADIR K, SAKAI T, UEHARA I. Structural investigation and hydrogen storage capacity of $LaMg_2Ni_9$ and $(La_{0.65}Ca_{0.35})(Mg_{1.32}Ca_{0.68})Ni_9$ of the AB_2C_9 type structure [J]. Journal of Alloys and Compounds, 2000, 302: 112−117.

[4] KADIR K, NOREUS D, YAMASHITA I. Structure determination of $AMgNi_4$ (where A=Ca, La, Ce, Pr, Nd and Y) in the $AuBe_5$ type structure [J]. Journal of Alloys and Compounds, 2002, 345: 140−143.

[5] BALCERZAK M, NOWAK M, JURCZYK M. Hydrogenation and electrochemical studies of La−Mg−Ni alloys [J]. International Journal of Hydrogen Energy, 2014, 42: 1436−1443.

[6] ZHANG Y H, REN H P, YANG T, ZHAO C, CHEN L C, SHANG H W. Electrochemical performances of as-cast and annealed $La_{0.8-x}Nd_xMg_{0.2}Ni_{3.35}Al_{0.1}Si_{0.05}$ (x=0−0.4) alloys applied to Ni/metal hydride (MH) battery [J]. Rare Metals, 2013, 32: 150−158.

[7] LIU Z P, YANG S Q, LI Y, LIU J J, MA M Z, HAN S M. Phase structure and electrochemical performances of Co-free La−Mg−Ni-based alloys with Nd/Sm partial substitution for La [J]. Rare Metals, 2014, 33: 674−680.

[8] LI Y, HAN D, HAN S M, ZHU X L, HU L, ZHANG Z, LIU Y W. Effect of rare earth elements on electrochemical properties of La−Mg−Ni-based hydrogen storage alloys [J]. International Journal of Hydrogen Energy, 2009, 34: 1399−1404.

[9] WANG Z M, ZHOU H Y, GU Z F, CHENG G, YU A B. Preparation of $LaMgNi_4$ alloy and its electrode properties [J]. Journal of Alloys and Compounds, 2004, 377: L7−L9.

[10] GUÉNÉE L, FAVRE-NICOLIN V, YVON K. Synthesis, crystal structure and hydrogenation properties of the ternary compounds $LaNi_4Mg$ and $NdNi_4Mg$ [J]. Journal of Alloys and Compounds, 2003, 348: 129−137.

[11] TIAN X, YUN G H, WANG H Y, SHANG T, YAO Z Q, WEI W, LIANG X X. Preparation and electrochemical properties of La−Mg−Ni-based $La_{0.75}Mg_{0.25}Ni_{3.3}Co_{0.5}$ multiphase hydrogen storage alloy as negative material of Ni/MH battery [J]. International Journal of Hydrogen Energy, 2014, 39: 8474−8481.

[12] TERESIAK A, UHLEMANN M, THOMAS J, ECKERT J, GEBERT A. Influence of Co and Pd on the formation of nanostructured $LaMg_2Ni$ and its hydrogen reactivity [J]. Journal of Alloys and Compounds, 2014, 582: 647−658.

[13] ZHANG Y H, YANG T, ZHAI T T, YUAN Z M, ZHANG G F, GUO S H. Effects of stoichiometric ratio La/Mg on structures and electrochemical performances of as-cast and annealed La−Mg−Ni-based A_2B_7-type electrode alloys [J]. Transactions of Nonferrous Metals Society of China, 2015, 25: 1968−1977.

[14] ZHANG Y H, HOU Z H, LI B W, REN H P, CAI Y, ZHAO D L. Electrochemical hydrogen storage characteristics of as-cast and annealed $La_{0.8-x}Nd_xMg_{0.2}Ni_{3.15}Co_{0.2}Al_{0.1}Si_{0.05}$ (x=0−0.4) alloys [J]. Transactions of Nonferrous Metals Society of China, 2013, 23: 1403−1412.

[15] YANG T, YUAN Z M, BU W G, JIA Z C, QI Y, ZHANG Y H. Effect of elemental substitution on the structure and hydrogen storage properties of $LaMgNi_4$ alloy [J]. Materials and Design, 2016, 93: 46−52.

[16] ZHANG Y H, ZHAO D L, SHI Y C, QI Y, GUO S H, WANG X L. Structures and electrochemical performances of $La_{0.75-x}Zr_xMg_{0.25}Ni_{3.2}Co_{0.2}Al_{0.1}$ (x=0−0.2) electrode alloys prepared by melt spinning [J]. Transactions of Nonferrous Metals Society of China, 2010, 20: 607−613.

[17] TERESIAK A, GEBERT A, SAVYAK M, UHLEMANN M, MICKEL C, MATTERN N. In situ high temperature XRD studies of the thermal behaviour of the rapidly quenched $Mg_{77}Ni_{18}Y_5$ alloy under hydrogen [J]. Journal of Alloys and Compounds, 2005, 398: 156−164.

[18] KURIYAMA N, SAKAI T, MIYAMURA H, UEHARA I, ISHIKAWA H, IWASAKI T. Electrochemical impedance and deterioration behavior of metal hydride electrodes [J]. Journal of Alloys and Compounds, 1993, 202: 183−197.

[19] DING H L, HAN H M, LIU Y, HAO J S, LI Y, ZHANG J W. Electrochemical performance studies on cobalt and nickel electroplated La–Mg–Ni-based hydrogen storage alloys [J]. International Journal of Hydrogen Energy, 2009, 34: 9402−9408.

[20] LAI W H, YU C Z. Research survey of improving discharge voltage platform for Ni−MH battery [J]. Battery Bimonthly, 1996, 26: 189−191. (in Chinese)

[21] WU Y, HAN W, ZHOU S X, LOTOTSKY M V, SOLBERG J K, YARTYS V A. Microstructure and hydrogenation behavior of ball-milled and melt-spun Mg−10Ni−2Mm alloys [J]. Journal of Alloys and Compounds, 2008, 466: 176−181.

[22] ORIMO S, FUJII H. Materials science of Mg−Ni-based new hydrides [J]. Applied Physics A, 2001, 72: 167−186.

[23] ZHAO X Y, DING Y, MA L Q, WANG L Y, YANG M, SHEN X D. Electrochemical properties of $MmNi_{3.8}Co_{0.75}Mn_{0.4}Al_{0.2}$ hydrogen storage alloy modified with nanocrystalline nickel [J]. International Journal of Hydrogen Energy, 2008, 33: 6727−6733.

[24] RUGGERI S, ROUÉ L, HUOT J, SCHULZ R, AYMARD L, TARASCON J M. Properties of mechanically alloyed Mg−Ni−Ti ternary hydrogen storage alloys for Ni−MH batteries [J]. Journal of Power Sources, 2002, 112: 547−556.

[25] ZHANG Y H, LI B W, REN H P, CAI Y, DONG X P, WANG X L. Cycle stabilities of the $La_{0.7}Mg_{0.3}Ni_{2.55-x}Co_{0.45}M_x$ (M=Fe, Mn, Al; x = 0, 0.1) electrode alloys prepared by casting and rapid quenching [J]. Journal of Alloys and Compounds, 2008, 458: 340−345.

[26] KLEPERIS J, WÓJCIK G, CZERWINSKI A, SKOWRONSKI J, KOPCAYK M, BELTOWSKA-BRZEZINSKA M. Electrochemical behavior of metal hydrides [J]. Journal of Solid State Electrochemistry, 2001, 5: 229−249.

[27] ZHANG G, POPOV B N, WHITE R E. Electrochemical determination of the diffusion coefficient of hydrogen through an $LaNi_{4.25}Al_{0.75}$ electrode in alkaline aqueous solution [J]. Journal of the Electrochemical Society, 1995, 142: 2695−2698.

[28] CUI N, LUO J L. Electrochemical study of hydrogen diffusion behavior in Mg_2Ni-type hydrogen storage alloy electrodes [J]. International Journal of Hydrogen Energy, 1999, 24: 37−42.

MH/Ni 电池用铸态及快淬态 RE−Mg−Ni−Co−Al 基合金的电化学储氢性能

张羊换[1,2]，李亚琴[2,3]，尚宏伟[2]，侯忠辉[1,2]，祁 焱[2]，赵栋梁[2]

1. 内蒙古科技大学 内蒙古自治区白云鄂博矿多金属资源综合利用重点实验室，包头 014010；
2. 钢铁研究总院 功能材料研究所，北京 100081；
3. 北京科技大学 新材料技术研究院, 北京 100083

摘 要：采用快淬方式制备 La−Mg−Ni−Co−Al 基 AB_2 型 $La_{0.8-x}Ce_{0.2}Y_xMgNi_{3.4}Co_{0.4}Al_{0.1}$ (x=0, 0.05, 0.1, 0.15, 0.2)合金。XRD、SEM 分析表明，实验合金包含主相 $LaMgNi_4$ 和第二相 $LaNi_5$。增加 Y 含量和淬速导致晶粒细化及相丰度明显改变，但不改变相组成。元素 Y 替代 La 元素和快淬使合金寿命明显改善，这归因于抗氧化、抗粉化和抗腐蚀能力的改善。另外，放电容量随 Y 含量的增加明显减小，而随淬速的增加先增加后下降。电化学动力学随淬速的增加先增加到最佳性能然后再下降。所有合金在第一次循环过程中就达到最大放电容量，不需要活化过程。

关键词：Y；La；替代；淬速；使用寿命；放电容量；电化学动力学

(Edited by Wei-ping CHEN)